

CONFIRMATION OF ONE OF THE COLDEST KNOWN BROWN DWARFS¹K. L. LUHMAN^{2,3}, A. J. BURGASSER⁴, I. LABBÉ⁵, D. SAUMON⁶, M. S. MARLEY⁷, J. J. BOCHANSKI², A. J. MONSON⁵, AND S. E. PERSSON⁵

Draft version February 25, 2024

ABSTRACT

Using two epochs of 4.5 μm images from the Infrared Array Camera (IRAC) on board the *Spitzer Space Telescope*, we recently identified a common proper motion companion to the white dwarf WD 0806-661 that is a candidate for the coldest known brown dwarf. To verify its cool nature, we have obtained images of this object at 3.6 μm with IRAC, at J with HAWK-I on the Very Large Telescope, and in a filter covering the red half of J with FourStar on Magellan. WD 0806-661 B is detected by IRAC but not HAWK-I or FourStar. From these data we measure colors of $[3.6] - [4.5] = 2.77 \pm 0.16$ and $J - [4.5] > 7.0$ (SNR < 3). Based on these colors and its absolute magnitudes, WD 0806-661 B is the coldest companion directly imaged outside of the solar system and is a contender for the coldest known brown dwarf with the Y dwarf WISEP J1828+2650. It is unclear which of these two objects is colder given the available data. A comparison of its absolute magnitude at 4.5 μm to the predictions of theoretical spectra and evolutionary models suggests that WD 0806-661 B has $T_{\text{eff}} = 300\text{--}345$ K.

Subject headings: binaries: visual — brown dwarfs — infrared: planetary systems — planetary systems — planets and satellites: atmospheres

1. INTRODUCTION

The coolest brown dwarfs are valuable laboratories for studies of the atmospheres and interiors of substellar objects, including gas giant planets. Recent years have seen significant progress in extending samples of brown dwarfs below 700 K ($\gtrsim T_8$). Many of these objects have been found at near-IR wavelengths through wide-field surveys (Warren et al. 2007; Delorme et al. 2008, 2010; Burningham et al. 2008, 2009, 2010; Lucas et al. 2010; Albert et al. 2011) and high-resolution imaging of substellar primaries (Liu et al. 2011a; Gelino et al. 2011). Because the coolest brown dwarfs are brightest at wavelengths longward of 4 μm (Burrows et al. 2003; Saumon & Marley 2008), a sensitive mid-IR telescope is the best tool for detecting them. One facility of this kind is the *Wide-field Infrared Survey Explorer* (*WISE*, Wright et al. 2010), which obtained mid-IR images of the entire sky in 2010. Data from *WISE* have already been used to dramatically increase the number of known late-T dwarfs (Mainzer et al. 2011; Burgasser et al. 2011; Scholz et al. 2011; Kirkpatrick et al. 2011; Liu et al. 2011b) and to discover the first objects that show clear

spectroscopic signatures of a new spectral class later than T (“Y dwarfs”, Cushing et al. 2011).

The *Spitzer Space Telescope* complements *WISE* by providing greater sensitivity for smaller fields (Werner et al. 2004). As a result, *Spitzer* is well-suited for finding brown dwarfs as companions to nearby stars (Luhman et al. 2007). To employ *Spitzer* for a companion survey, we have searched multi-epoch *Spitzer* images for objects that are comoving with stars in the solar neighborhood. Through this work, we recently identified a common proper motion companion to the white dwarf WD 0806-661 (Luhman et al. 2011). The 4.5 μm absolute magnitude of WD 0806-661 B suggests that it could be the faintest and coolest known brown dwarf ($T_{\text{eff}} \sim 300$ K). In addition to potentially breaking new ground in terms of temperature, this companion could be one of a small number of benchmark brown dwarfs whose ages are known via their primaries and thus can provide unusually stringent tests of theoretical models of substellar objects. However, the temperature of WD 0806-661 B is uncertain since it has been detected at only 4.5 μm .

To confirm its substellar nature and better constrain its temperature, we have obtained deep near- and mid-IR images of WD 0806-661 B with *Spitzer* and ground-based telescopes. In this paper, we describe the collection and reduction of these data (Section 2), use the resulting astrometry and photometry to assess the companionship and properties of WD 0806-661 B (Section 3), and discuss the implications of this object for theoretical models and surveys for cool brown dwarfs (Section 4).

2. OBSERVATIONS

2.1. *Spitzer* IRAC

WD 0806-661 B was imaged previously at 4.5 μm by the Infrared Array Camera (IRAC; Fazio et al. 2004) on board *Spitzer* in 2004 and 2009, as described by Luhman et al. (2011). To measure a color relative to 4.5 μm that is sensitive to temperature for cool brown

¹ Based on observations made with the following facilities: the *Spitzer Space Telescope*, which is operated by the Jet Propulsion Laboratory, California Institute of Technology under a contract with NASA; the ESO Telescopes at Paranal Observatory under program ID 286.C-5042; the 6.5 meter Magellan Telescopes located at Las Campanas Observatory, Chile.

² Department of Astronomy and Astrophysics, The Pennsylvania State University, University Park, PA 16802, USA; kluhman@astro.psu.edu

³ Center for Exoplanets and Habitable Worlds, The Pennsylvania State University, University Park, PA 16802, USA

⁴ Center for Astrophysics and Space Science, University of California San Diego, La Jolla, CA 92093, USA

⁵ Observatories of the Carnegie Institution for Science, 813 Santa Barbara St., Pasadena, CA 91101, USA

⁶ Los Alamos National Laboratory, P.O. Box 1663, MS F663, Los Alamos, NM 87545, USA

⁷ Space Science and Astrobiology Division, NASA Ames Research Center, Mail Stop 245-3, Moffett Field, CA 94035, USA

dwarfs, we elected to observe WD 0806-661 B at $3.6\ \mu\text{m}$ with IRAC (Patten et al. 2006). This camera has a plate scale and a field of view of $1''.2\ \text{pixel}^{-1}$ and $5''.2 \times 5''.2$, respectively, and produces images with $\text{FWHM} = 1''.6$ at $3.6\ \mu\text{m}$. On 2011 April 18, IRAC collected one 93.6 s exposure of WD 0806-661 B through the $3.6\ \mu\text{m}$ filter at each position in a 12-point dither pattern. These observations were conducted through Astronomical Observation Request 41905408 for program 70203.

The Spitzer Science Center pipeline (version S18.18.0) performed the initial processing of the individual $3.6\ \mu\text{m}$ images. We then combined these images into one mosaic using the Overlap and Mosaic pipelines within the Mosaicking and Point-source Extraction software package (MOPEX, Makovoz & Marleau 2005). We used MOPEX rather than the software applied to the $4.5\ \mu\text{m}$ data by Luhman et al. (2011) since it offers drizzling and Point Response Function (PRF) subtraction, which are beneficial for our analysis of WD 0806-661 B, as described below. We re-reduced the two sets of $4.5\ \mu\text{m}$ images with MOPEX as well. A plate scale of $0''.6\ \text{pixel}^{-1}$ was selected for the final mosaics. To optimize the accuracy of the relative astrometry between the three mosaics, we measured new world coordinate systems (WCSs) for the first and third epochs of data based on the second epoch mosaic in the manner described by Luhman et al. (2011).

The reduced IRAC images surrounding the position of WD 0806-661 B are shown in Figure 1. We indicate the detections of the companion in the first two epochs at $4.5\ \mu\text{m}$. WD 0806-661 B is detected in the new image at $3.6\ \mu\text{m}$ at the location expected based on its astrometry and proper motion from the $4.5\ \mu\text{m}$ data (Section 3.1), although it is much fainter than at $4.5\ \mu\text{m}$. In the $3.6\ \mu\text{m}$ image, WD 0806-661 B is partially blended with another source at a distance of $\sim 2''$ that is similar in brightness, which is presumably a background star or galaxy. The use of drizzling within MOPEX has optimized the spatial resolution of the final mosaic, making it slightly easier to resolve WD 0806-661 B from this source. Through the Apex pipeline within MOPEX, we applied PRF fitting to the pair of objects and subtracted the fit to the background source, as shown in Figure 1. The background object also is visible in the wing of WD 0806-661 B in the second $4.5\ \mu\text{m}$ image, but because WD 0806-661 B is much brighter at that wavelength, we did not notice its presence in Luhman et al. (2011). We have now attempted to subtract the contribution from this source in this $4.5\ \mu\text{m}$ image in the same manner as done at $3.6\ \mu\text{m}$. The aperture for photometry of WD 0806-661 B in the first epoch at $4.5\ \mu\text{m}$ does not encompass the location of the background source.

We measured aperture photometry for WD 0806-661 B in each of the three mosaics with an aperture radius of 4 pixels ($2''.4$) and radii of 5 and 10 pixels for the inner and outer boundaries of the sky annulus, respectively. To estimate aperture corrections, we measured photometry for all sources in a given mosaic with these parameters and with those used by Luhman et al. (2010), computed the average offset between the two sets of photometry, and combined this offset with the aperture corrections measured by Luhman et al. (2010). We present the resulting photometry at 3.6 and $4.5\ \mu\text{m}$ in Table 1. Our new measurements at $4.5\ \mu\text{m}$ is fainter than the value we

reported in Luhman et al. (2011) because of the subtraction of the blended background source from the second epoch data.

2.2. VLT HAWK-I

In addition to the $3.6\ \mu\text{m}$ data from IRAC, we have pursued near-IR photometry to further constrain the temperature of WD 0806-661 B and to assess the feasibility of spectroscopy. We have focused on filters near $1.2\text{--}1.3\ \mu\text{m}$ (e.g., J) for these observations since they offer the best sensitivity at near-IR wavelengths for cool brown dwarfs. Our first set of near-IR images was obtained with the High Acuity Wide-field K-band Imager (HAWK-I) on the Unit Telescope 4 of the Very Large Telescope (VLT). This camera contains four 2048×2048 HAWAII-2RG arrays and has a plate scale of $0''.106\ \text{pixel}^{-1}$ (Kissler-Patig et al. 2008). During the nights of 2011 March 5 and 6, WD 0806-661 B was placed within one of the four arrays and 47 dithered images were collected, each of which consisted of 15 coadded 6.2 s exposures. Thus, the total exposure time was 72.85 min. These observations were performed through program 286.C-5042.

For each of the HAWK-I images from the array containing WD 0806-661 B, we subtracted a dark frame and divided by a flat field image. The resulting images were registered and combined into a single mosaic. To measure the WCS and flux calibration for the mosaic, we began by reducing archival J -band images of this field that are publicly available from the Infrared Side Port Imager at the 4 m Blanco telescope (Rodriguez et al. 2011). We used astrometry and photometry from the Point Source Catalog of the Two-Micron All-Sky Survey (2MASS, Skrutskie et al. 2006) to measure the flux calibration and WCS of the ISPI mosaic, which is large enough ($10' \times 10'$) to encompass a sufficient number of 2MASS sources. We then used ISPI astrometry and photometry to determine the WCS and flux calibration of the HAWK-I data.

Point sources in the HAWK-I mosaic exhibit $\text{FWHM} \sim 0''.7$. To facilitate visual detection of sources with low signal-to-noise ratios (SNRs) in Figure 1, we have smoothed the image to a resolution of $1''$. WD 0806-661 B is not detected in this image. We estimate that $\text{SNR}=3$ corresponds to $J \sim 23.9$.

2.3. Magellan FourStar

We obtained a second set of near-IR images of WD 0806-661 B using FourStar on the Magellan 6.5 m Baade Telescope. This camera employs four 2048×2048 HAWAII-2RG arrays and has a plate scale of $0''.159\ \text{pixel}^{-1}$ (Persson et al. 2008). We used a medium-band filter (denoted as $J3$) that extends from $1.22\text{--}1.35\ \mu\text{m}$ rather than a standard J -band filter ($1.13\text{--}1.35\ \mu\text{m}$) since it is aligned more closely with the wavelengths at which the near-IR fluxes of T dwarfs are highest. During the nights of 2011 April 17 and 18, we placed WD 0806-661 B in one of the four arrays of FourStar and collected 46 dithered images, each of which consisted of three coadded 32 s exposures. The resulting total exposure time was 73.6 min.

The FourStar images were reduced with procedures similar to those applied to the HAWK-I data. We derived the flux calibration of the final mosaic from images of two

photometric standards, GD71 and GD173, and synthetic $J - J3$ Vega-based colors derived from the transmission profiles for these filters. To verify this calibration, we also calibrated the mosaic using the ISPI photometry as done for HAWK-I. The ISPI sources that appear within the FourStar data have a mean color of $J - H \sim 0.5$. Using a spectrum of Vega, we estimate that an A0V star reddened to have this color will have $J - J3 \sim 0.1$. When we combined this color with the ISPI J -band photometry for sources detected by FourStar, we arrived at the same flux calibration as derived from the photometric standards.

The average FWHM for point sources in the FourStar mosaic is $\sim 0''.75$. As with the HAWK-I data, we have smoothed the FourStar image to a resolution of $1''$ for display in Figure 1, and it does not show a detection of WD 0806-661 B. We estimate that $\text{SNR}=3$ corresponds to a Vega-based magnitude of $J3 \sim 23.5$ in this image. By combining the observed spectra of late T dwarfs with the transmission profiles for J and $J3$, we derive colors of $J - J3 \sim 0.4$. When we use the model spectra of brown dwarfs from Burrows et al. (2003) and Saumon & Marley (2008), we arrive at similar values of $J - J3$ for temperatures above 250 K. Thus, the limit of $J3 \gtrsim 23.5$ implies that WD 0806-661 B has $J \gtrsim 23.9$, which is the same as the limit measured with HAWK-I.

Luhman et al. (2011) and Rodriguez et al. (2011) have previously reported J -band limits for WD 0806-661 B. Rodriguez et al. (2011) measured a limit of $J > 21.7$ for $\text{SNR}<3$, which they described as 1.7 mag fainter than the one from Luhman et al. (2011). However, the two limits were not compared at the same SNR. Given that the limit of $J > 20$ from Luhman et al. (2011) corresponded to $\text{SNR}>10$, the J -band constraint from Rodriguez et al. (2011) was 0.4 mag deeper than that from Luhman et al. (2011).

3. ANALYSIS

3.1. Common Proper Motion

Luhman et al. (2011) identified WD 0806-661 B as a companion based on its common proper motion with the primary between the first two epochs of IRAC images. Given our new detection of WD 0806-661 B at $3.6 \mu\text{m}$, we can verify that WD 0806-661 B shares the same proper motion as the primary. In Figure 2, we show the differences in equatorial coordinates between the $3.6 \mu\text{m}$ image and the first $4.5 \mu\text{m}$ image for stars detected in both images. To estimate the uncertainty in the displacement of the secondary, one would normally examine the scatter in Figure 2 for sources near its magnitude. However, because WD 0806-661 B is very red in $[3.6] - [4.5]$, few sources in the IRAC images match its brightness at both wavelengths. As an alternative means of estimating the uncertainties, we have computed the standard deviations of the differences in right ascension and declination for objects that have a similar combination of SNRs, except in the opposite bands compared to WD 0806-661 B. In other words, whereas WD 0806-661 B has a low SNR at $3.6 \mu\text{m}$ and a high SNR in $4.5 \mu\text{m}$, we have considered sources that have low and high SNRs at 4.5 and $3.6 \mu\text{m}$, respectively. Many sources of this kind are available because the $3.6 \mu\text{m}$ images are deeper than the $4.5 \mu\text{m}$ data. In this way, we estimate a 1σ uncertainty of $0''.25$

in each of the offsets in right ascension and declination. As demonstrated in Figure 2, the motion of WD 0806-661 B based on our new astrometry is non-zero at a level of 8σ in each direction and is consistent within $\sim 1 \sigma$ of that of the primary.

3.2. Photometric Properties

WD 0806-661 B was detected only at $4.5 \mu\text{m}$ in previous images. As a result, only limits were available for its colors, such as $J - [4.5]$, which strongly suggested a cool temperature (Luhman et al. 2011; Rodriguez et al. 2011). Our detection at $3.6 \mu\text{m}$ now provides a direct measurement of a color for WD 0806-661 B. We find that it has $[3.6] - [4.5] = 2.77 \pm 0.16$, which is much redder than the neutral colors exhibited by most astronomical sources and confirms that it is a cool, methane-bearing object (Patten et al. 2006).

To investigate how WD 0806-661 B compares to previously known brown dwarfs in terms of temperature and luminosity, we begin by constructing diagrams of $M_{4.5}$ versus $[3.6] - [4.5]$ and $M_{4.5}$ versus $J - [4.5]$ in Figure 3 for WD 0806-661 B and all known T and Y dwarfs that have measured distances and IRAC photometry (Lucas et al. 2010; Leggett et al. 2010; Burningham et al. 2011; Kirkpatrick et al. 2011, references therein). We have adopted the J -band photometry compiled by Leggett et al. (2010) and Kirkpatrick et al. (2011) and have plotted separately the data from the 2MASS and Mauna Kea Observatories (MKO) systems. Sources that have been observed in both systems are plotted twice. When multiple J -band measurements are available for a given object, we have adopted the mean of those data weighted by the inverse square of their flux errors. In Figure 3, WD 0806-661 B is redder and fainter than all of the T dwarfs in this sample. It is also redder than the one Y dwarf with a measured parallax, WISEP J154151.65-225025.2 (hereafter WISEP J1541-2250, Cushing et al. 2011; Kirkpatrick et al. 2011), but that object appears to be fainter than WD 0806-661 B. As a result, a single sequence of T and Y dwarfs would not be pass through the locations of both WD 0806-661 B and WISEP J1541-2250 in the color-magnitude diagrams, unless the former is an unresolved binary. This discrepancy may arise from the large uncertainty in the parallax of WISEP J1541-2250. We note that the very cool brown dwarf companion CFBDSIR J1458+1013 B is absent from Figure 3 since it lacks mid-IR photometry. It is $\gtrsim 10$ times brighter than WD 0806-661 B in M_J , and hence should be significantly warmer (Table 1, Liu et al. 2011a).

Since *WISE* has also measured mid-IR data for a large number of brown dwarfs, we have included in Figure 3 color-magnitude diagrams based on the *WISE* bands at 3.4 and $4.6 \mu\text{m}$ (denoted as $W1$ and $W2$). These data are from Mainzer et al. (2011), Burgasser et al. (2011), Cushing et al. (2011), and Kirkpatrick et al. (2011). The photometry from the $W2$ and IRAC $4.5 \mu\text{m}$ filters have an average offset of less than a few percent for L and T dwarfs while the $W1$ magnitudes are fainter than those from IRAC $3.6 \mu\text{m}$ by an average of ~ 0.5 to 1.5 mag from early T dwarfs to Y dwarfs (Kirkpatrick et al. 2011).

In Figure 4, we expand our comparison to include known T and Y dwarfs that lack distance estimates by constructing diagrams that contain only colors and spec-

tral types. We present diagrams based on both IRAC and *WISE* photometry. As shown in Figure 4, WD 0806-661 B is as red as or redder than all known T and Y dwarfs in $[3.6] - [4.5]$ and $J - [4.5]$, with the possible exception of WISEP J1828+2650. WD 0806-661 B is marginally redder than that Y dwarf in $[3.6] - [4.5]$, but it is unknown how they compare in $J - [4.5]$. WD 0806-661 B is also redder in $[3.6] - [4.5]$ than all of the late T candidates found in the *Spitzer* Deep, Wide-Field Survey (Eisenhardt et al. 2010).

3.3. Physical Properties

We can use our new photometry for WD 0806-661 B to update our previous estimates of its mass and effective temperature from Luhman et al. (2011). To derive the mass of WD 0806-661 B, Luhman et al. (2011) compared $M_{4.5}$ to the predictions of evolutionary models for the age of the primary. In that study, our age estimate was in part based on an analytic relation between initial stellar mass and evolutionary time through the end of core helium burning (Iben & Laughlin 1989). We now revise our previous calculation to use the evolutionary time predicted by the numerical models from Girardi et al. (2002), which results in a new estimate of 2 ± 0.5 Gyr for the total age of the white dwarf. When we compare our new measurement of $M_{4.5}$ to the values predicted by Burrows et al. (2003) and Saumon & Marley (2008) for this age, we arrive at a mass of 6–9 M_{Jup} for WD 0806-661 B.

Both the colors and absolute magnitudes of cool brown dwarfs are sensitive to their temperatures. To assess which of these measurements for WD 0806-661 B is most likely to produce a reliable temperature estimate, we have plotted theoretical colors and magnitudes of brown dwarfs in Figure 3 for ages of 1 and 3 Gyr. We have considered the cloudy models from Burrows et al. (2003), which employ equilibrium chemistry, and new versions of the cloudless models from Saumon & Marley (2008) for both equilibrium and non-equilibrium chemistry. The new models based on Saumon & Marley (2008) include updates to the ammonia and hydrogen collision induced absorption opacities (Yurchenko et al. 2011; Frommhold et al. 2010) and an extension to lower effective temperatures. The non-equilibrium models are computed with an eddy diffusion coefficient of $K_{zz} = 10^4 \text{ cm}^2 \text{ s}^{-1}$. As shown in Figure 3, all of the models are much redder than known T dwarfs in $[3.6] - [4.5]$ and the equivalent color from *WISE*. Leggett et al. (2009, 2010) found a similar discrepancy in the values of $[3.6] - [4.5]$ predicted by Saumon & Marley (2008), which they attributed to errors in the model fluxes at $3.6 \mu\text{m}$. The models agree reasonably well with the observed sequence of T dwarfs in $M_{4.5}$ versus $J - [4.5]$. Both sets of equilibrium models are consistent with the location of WD 0806-661 B in $M_{4.5}$ versus $J - [4.5]$ while the non-equilibrium calculations produce a value of $J - [4.5]$ that is slightly too blue. Therefore, we rely on $J - [4.5]$ and $M_{4.5}$ for estimating the temperature of WD 0806-661 B.

In Figure 5, we compare the constraints on $J - [4.5]$ and $M_{4.5}$ to the values predicted as a function of effective temperature by the models. The limit of $J - [4.5] > 7.0$ implies $T_{\text{eff}} \lesssim 320$ K and $T_{\text{eff}} \lesssim 355$ K for WD 0806-661 B based on the calculations of Burrows et al. (2003) and Saumon & Marley (2008),

respectively. Using $M_{4.5} = 15.47 \pm 0.09$, we derive $T_{\text{eff}} = 310 \pm 10$ K with Burrows et al. (2003) and $T_{\text{eff}} = 325 \pm 10$ K with Saumon & Marley (2008). The models for these temperature estimates assume chemical equilibrium. The temperatures implied by $J - [4.5]$ and $M_{4.5}$ using the non-equilibrium models are marginally inconsistent with each other ($T_{\text{eff}} \lesssim 325$ K, $T_{\text{eff}} = 340 \pm 5$ K), which is a reflection of the fact that these models do not pass through the location of WD 0806-661 B in Figure 3. The quoted uncertainties represent only the error in $M_{4.5}$ and do not include the unknown systematic errors in the model predictions.

We now examine the temperature of WD 0806-661 B in the context of one of the faintest known brown dwarfs, CFBDSIR J1458+1013 B. Liu et al. (2011a) considered two methods for estimating the temperature of this object. In the first one, they found $T_{\text{eff}} \sim 400$ K for CFBDSIR J1458+1013 B by comparing M_J to the predictions of Burrows et al. (2003), which is similar to our approach for WD 0806-661 B. Liu et al. (2011a) also compared the bolometric luminosity to the values from evolutionary models, which produced a lower temperature of ~ 350 – 380 K. To estimate the luminosity of CFBDSIR J1458+1013 B, they assumed that it has the same J -band bolometric correction (BC_J) as T dwarfs at 500–600 K. However, BC_J is expected to change by ~ 1.4 mag between 500–600 K and 350–400 K according to the models of Burrows et al. (2003) and Saumon & Marley (2008). The rapid increase in $J - [4.5]$ that is observed at lower temperatures (Figure 4) also indicates that BC_J is unlikely to remain constant. As a result, the bolometric luminosity of CFBDSIR J1458+1013 B was probably underestimated, which would explain why the luminosity-based temperature was lower than the value derived from M_J .

4. DISCUSSION

Through deep imaging at J and $3.6 \mu\text{m}$, we have further demonstrated the companionship of WD 0806-661 B via its common proper motion with its primary and have provided new constraints on its photometric properties. We have found that WD 0806-661 B is redder than at least five of the six Y dwarfs recently discovered by Cushing et al. (2011), indicating that it is probably a member of this new spectral class as well. WD 0806-661 B and the Y dwarf WISEP J1828+2650 appear to be the coldest known brown dwarfs based on their $[3.6] - [4.5]$ and $J - [4.5]$ colors. A J -band detection of WD 0806-661 B and a parallax measurement for WISEP J1828+2650 are needed to determine their relative temperatures. More accurate photometry at $3.6 \mu\text{m}$ for the former and at J for the latter also would help refine the comparison of these objects.

In addition to representing one of the coldest known objects directly observed outside the solar system, WD 0806-661 B is a benchmark for testing atmospheric and evolutionary models at substellar masses since its age and distance are well-constrained via its primary. To fully exploit it for this purpose, deeper imaging at J and other bands is necessary. WD 0806-661 B is too faint for ground-based spectroscopy, but near-IR grism observations with the *Hubble Space Telescope* may be feasible. The new Y dwarfs found with *WISE* have closer distances and are much more amenable to detailed spec-

troscopic study (Cushing et al. 2011), but even low-SNR spectroscopy of WD 0806-661 B would be valuable given its extreme temperature and benchmark status.

Because of the rapid decrease in the J -band fluxes of brown dwarfs at the lowest temperatures, it seems unlikely that objects cooler than WD 0806-661 B will be found with wide-field ground-based imaging, which is restricted to near-IR wavelengths. For instance, current ground-based surveys have identified T dwarfs down to $J \sim 19.5$ (Burningham et al. 2010; Delorme et al. 2010), corresponding to a distance limit of < 2.5 pc for analogs of WD 0806-661 B. The discovery of any additional objects with $T_{\text{eff}} \lesssim 350$ K over the next decade will probably occur through continued analysis of mid-IR data from the *WISE* and *Spitzer* satellites. For instance, typical mid-IR images from *WISE* are capable of detecting objects like WD 0806-661 B with SNR=10 out to distances of ~ 7 pc. It also is possible that companions in this temperature regime could be uncovered through very deep near-IR imaging of the nearest stars with ground-based adaptive optics or the *Hubble Space Telescope*.

We acknowledge support from grant AST-0544588 from the National Science Foundation (K. L., J. B.) and the NASA Astrophysics Theory Program (M. M., D. S.). This publication makes use of data products from the following resources: the *Wide-field Infrared Survey Explorer*, which is a joint project of the University of California, Los Angeles, and the Jet Propulsion Laboratory/California Institute of Technology, funded by the National Aeronautics and Space Administration; the NASA/IPAC Infrared Science Archive, which is operated by the Jet Propulsion Laboratory, California Institute of Technology, under contract with the National Aeronautics and Space Administration; the SpeX Prism Spectral Libraries, maintained by Adam Burgasser at <http://www.browndwarfs.org/spexprism>; the M, L, and T dwarf compendium housed at <http://DwarfArchives.org> and maintained by Chris Gelino, Davy Kirkpatrick, and Adam Burgasser. The Center for Exoplanets and Habitable Worlds is supported by the Pennsylvania State University, the Eberly College of Science, and the Pennsylvania Space Grant Consortium.

REFERENCES

- Albert, L., Étienne, A., Delorme, P., et al. 2011, *AJ*, 141, 203
 Burgasser, A. J., Cushing, M. C., Kirkpatrick, J. D., et al. 2011, *ApJ*, 735, 116
 Burningham, B., Pinfield, D. J., Leggett, S. K., et al. 2008, *MNRAS*, 391, 320
 Burningham, B., Pinfield, D. J., Leggett, S. K., et al. 2009, *MNRAS*, 395, 1237
 Burningham, B., Pinfield, D. J., Lucas, P. W., et al. 2010, *MNRAS*, 406, 1885
 Burningham, B., Leggett, S. K., Homeier, D., et al. 2011, *MNRAS*, 414, 3590
 Burrows, A., Sudarsky, D., & Lunine, J. I. 2003, *ApJ*, 596, 587
 Cushing, M. C., et al. 2011, *ApJ*, in press
 Delorme, P., Delfosse, X., Albert, L., et al. 2008, *A&A*, 482, 961
 Delorme, P., Albert, L., Forveille, T., et al. 2010, *A&A*, 518, A39
 Eisenhardt, P. R. M., Griffith, R. L., Stern, D., et al. 2010, *AJ*, 139, 2455
 Fazio, G. G., Hora, J. L., Allen, L. E., et al. 2004, *ApJS*, 154, 10
 Frommhold, L., Abel, F., Wang, M., et al. 2010, *Molecular Physics*, 108, 2265
 Gelino, C. R., Kirkpatrick, J. D., Cushing, M. C., et al. 2011, *AJ*, 142, 57
 Girardi, L., Bertelli, G., Bressan, A., et al. 2002, *A&A*, 391, 195
 Iben, I., Jr., & Laughlin, G. 1989, *ApJ*, 341, 312
 Kirkpatrick, J. D., et al. 2011, *ApJS*, in press
 Kissler-Patig, M., Pirard, J.-F., Casali, M., et al. 2008, *A&A*, 491, 941
 Leggett, S. K., Cushing, M. C., Saumon, D., et al. 2009, *ApJ*, 695, 1517
 Leggett, S. K., Burningham, B., Saumon, D., et al. 2010, *ApJ*, 710, 1627
 Lucas, P. W., Tinney, C. G., Burningham, B., et al. 2010, *MNRAS*, 408, L56
 Liu, M. C., Delorme, P., Dupuy, T. J., et al. 2011a, *ApJ*, 740, L32
 Liu, M. C., Deacon, N. R., Magnier, E. A., et al. 2011b, *ApJ*, 740, 108
 Luhman, K. L., Allen, P. R., Espaillat, C., Hartmann, L., & Calvet, N. 2010, *ApJS*, 186, 111
 Luhman, K. L., Burgasser, A. J., & Bochanski, J. J. 2011, *ApJ*, 730, L9
 Luhman, K. L., Patten, B. M., Marengo, M., et al. 2007, *ApJ*, 654, 570
 Mainzer, A., Cushing, M. C., Skrutskie, M., et al. 2011, *ApJ*, 726, 30
 Makovoz, D., & Marleau, F. R. 2005, *PASP*, 117, 1113
 Patten, B. M., Stauffer, J. R., Burrows, A., et al. 2006, *ApJ*, 651, 502
 Persson, S. E., Barkhouser, R., Birk, C., et al. 2008, *Proc. SPIE*, 7014, 95
 Rodriguez, D. R., Zuckerman, B., Melis, C., & Song, I. 2011, *ApJ*, 732, L29
 Saumon, D., & Marley, M. S. 2008, *ApJ*, 689, 1327
 Scholz, R.-D., Bihain, G., Schnurr, O., & Storm, J. 2011, *A&A*, 532, L5
 Skrutskie, M., Cutri, R. M., Stiening, R., et al. 2006, *AJ*, 131, 1163
 Subasavage, J. P., Jao, W.-C., Henry, T. J., et al. 2009, *AJ*, 137, 4547
 Warren, S. J., Mortlock, D. J., Leggett, S. K., et al. 2007, *MNRAS*, 381, 1400
 Werner, M. W., Roellig, T. L., Low, F. J., et al. 2004, *ApJS*, 154, 1
 Wright, E. L., Eisenhardt, P. R. M., Mainzer, A. K., et al. 2010, *AJ*, 140, 1868
 Yurchenko, S. N., Barber, R. J., & Tennyson, J. 2011, *MNRAS*, 413, 1828

TABLE 1
PROPERTIES OF
WD 0806-661 B

Parameter	Value
Distance	19.2 ± 0.6 pc ^a
Age	2 ± 0.5 Gyr ^b
J	> 23.9 ^c
$J3$	> 23.5 ^{c,d}
[3.6]	19.65 ± 0.15
[4.5] (2004)	16.96 ± 0.09
[4.5] (2009)	16.84 ± 0.06
[4.5] (mean)	16.88 ± 0.05
$M_{4.5}$	15.47 ± 0.09
T_{eff}	$300\text{--}345$ K ^e
Mass	$6\text{--}9$ M_{Jup} ^e

^a Measured for the primary (Subasavage et al. 2009).

^b Estimated for the primary (Section 3.3).

^c $\text{SNR} < 3$.

^d WD 0806-661 B likely has $J - J3 \sim 0.4$.

^e Based on a comparison of M_J and $J - [4.5]$ to the values predicted by the models in Figure 5.

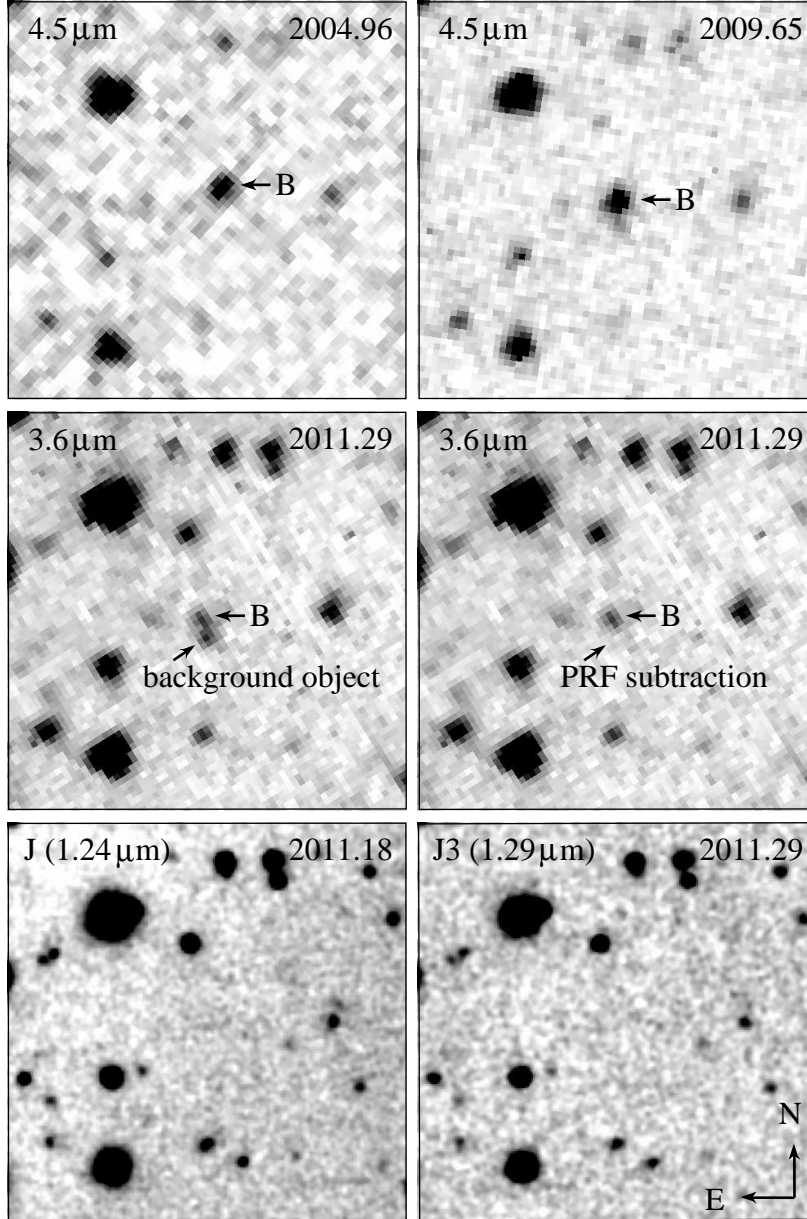


FIG. 1.— Discovery images of WD 0806-661 B at 4.5 μm (Luhman et al. 2011) and new data at 3.6 μm , J (1.24 μm), and $J3$ (1.29 μm). WD 0806-661 B is detected at 3.6 μm but not in J and $J3$. It is partially blended with a background object in the 3.6 μm image. We have applied PRF subtraction to the latter prior to measuring astrometry and photometry for WD 0806-661 B. The size of each image is $40'' \times 40''$.

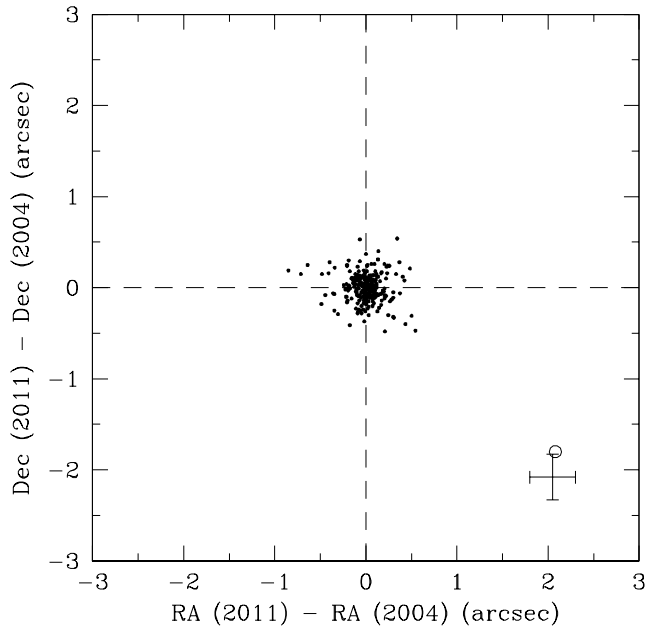


FIG. 2.— Differences in coordinates between the *Spitzer* IRAC images from 2004 and 2011 for WD 0806-661 (circle), its companion (1σ error bars), and all other sources (points).

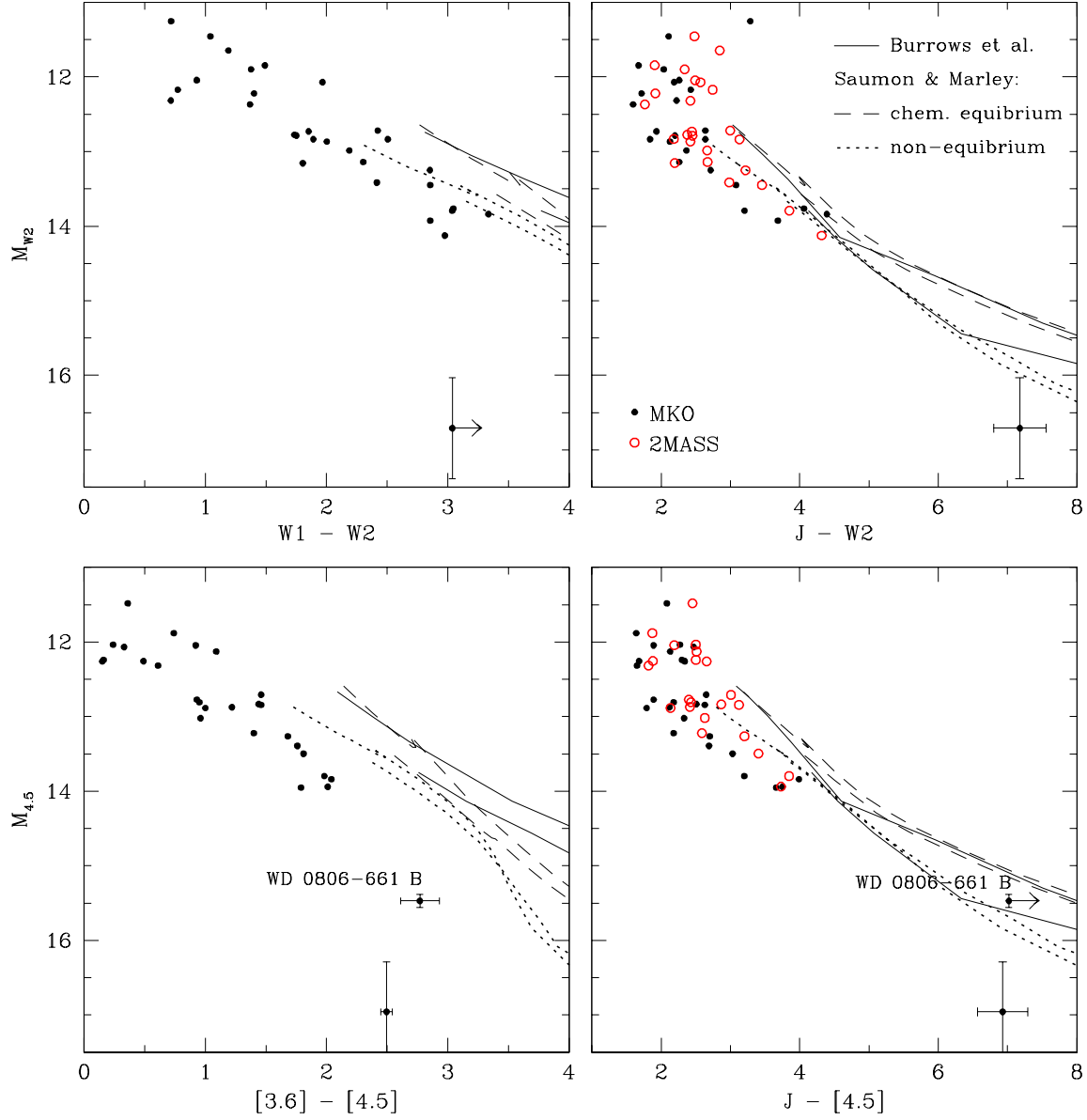


FIG. 3.— Color-magnitude diagrams for known T and Y dwarfs with measured distances based on data from *WISE* and IRAC on *Spitzer* (top and bottom, Lucas et al. 2010; Leggett et al. 2010; Cushing et al. 2011; Kirkpatrick et al. 2011, references therein). Our data for WD 0806-661 B are indicated in the bottom diagrams. Error bars are included for WD 0806-661 B and the Y dwarf WISEP J1541-2250. For comparison, we show the magnitudes and colors predicted for ages of 1 and 3 Gyr by the theoretical spectra and evolutionary models from Burrows et al. (2003, solid lines) and Saumon & Marley (2008, dashed and dotted lines).

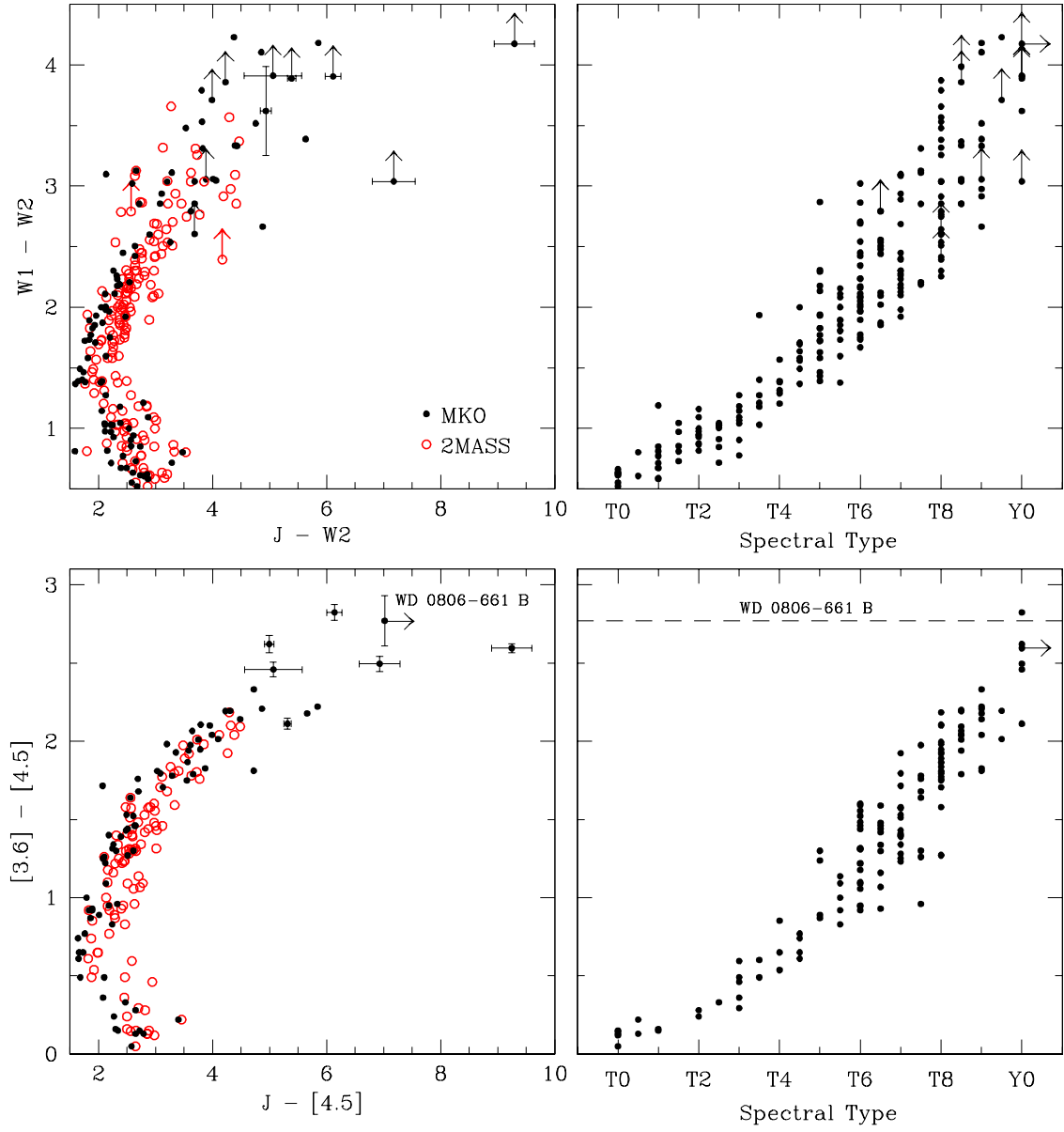


FIG. 4.— Color-color diagrams and colors versus spectral type for known T and Y dwarfs based on data from *WISE* and IRAC on *Spitzer* (top and bottom, Lucas et al. 2010; Leggett et al. 2010; Burningham et al. 2011; Cushing et al. 2011; Kirkpatrick et al. 2011, references therein). Our data for WD 0806-661 B are indicated in the bottom diagrams. Error bars are included in the left diagrams for WD 0806-661 B and the Y dwarfs.

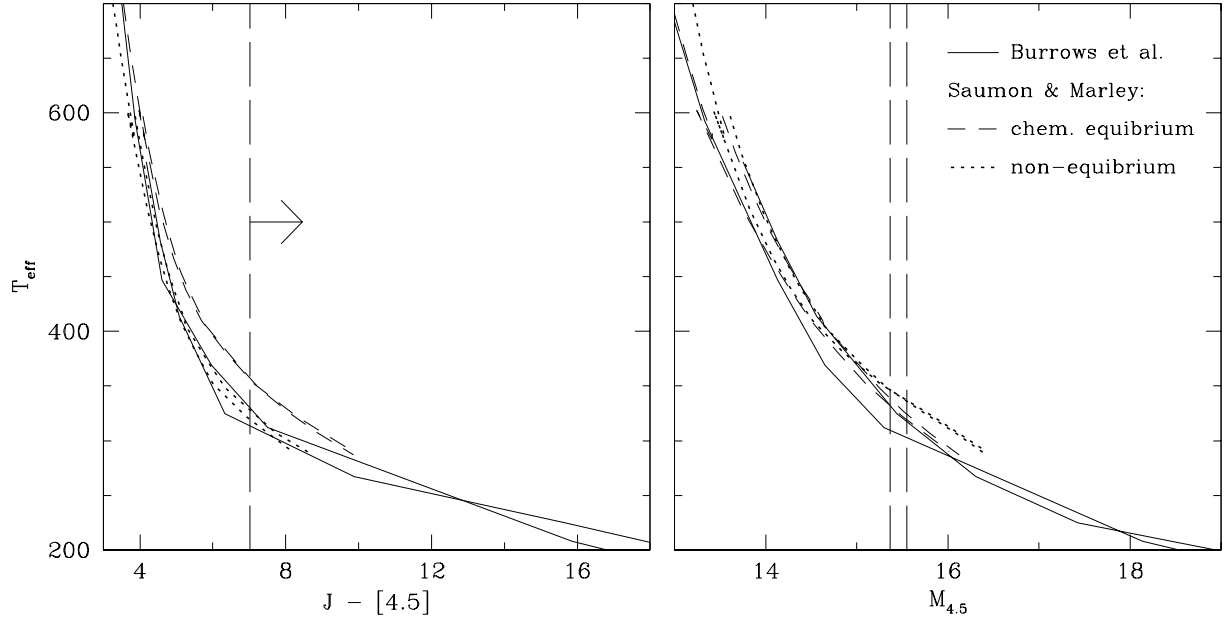


FIG. 5.— Predicted $J - [4.5]$ and $M_{4.5}$ as a function of effective temperature based on the models from Burrows et al. (2003, solid lines) and Saumon & Marley (2008, short dashed and dotted lines) for ages of 1 and 3 Gyr. The constraints on $J - [4.5]$ and $M_{4.5}$ for WD 0806-661 B are indicated (long dashed lines).